



# First principles study of structural, optoelectronic and photocatalytic properties of SnS, SnSe monolayers and their van der Waals heterostructure

Thi-Nga Do<sup>a,b</sup>, M. Idrees<sup>c</sup>, Bin Amin<sup>d</sup>, Nguyen N. Hieu<sup>e,f</sup>, Huynh V. Phuc<sup>g</sup>, Le T. Hoa<sup>e,f,\*</sup>,  
Chuong V. Nguyen<sup>h</sup>

<sup>a</sup> Laboratory of Magnetism and Magnetic Materials, Advanced Institute of Materials Science, Ton Duc Thang University, Ho Chi Minh City, Viet Nam

<sup>b</sup> Faculty of Applied Sciences, Ton Duc Thang University, Ho Chi Minh City, Viet Nam

<sup>c</sup> Department of Physics, Hazara University, Mansehra 21300, Pakistan

<sup>d</sup> Department of Physics, Abbottabad University of Science and Technology, Abbottabad 22010, Pakistan

<sup>e</sup> Institute of Research and Development, Duy Tan University, Da Nang 550000, Viet Nam

<sup>f</sup> Faculty of Natural Sciences, Duy Tan University, Da Nang 550000, Viet Nam

<sup>g</sup> Division of Theoretical Physics, Dong Thap University, Cao Lanh 870000, Viet Nam

<sup>h</sup> Department of Materials Science and Engineering, Le Quy Don Technical University, Ha Noi 100000, Viet Nam

## ARTICLE INFO

### Keywords:

2D materials  
van der Waals heterostructure  
photocatalytic performance  
DFT calculations

## ABSTRACT

Electronic structure, optical, and photocatalytic properties of SnS, SnSe and their van der Waals heterostructures are investigated by first-principle calculations. Thermal stability confirmed that SnS, SnSe and SnS-SnSe van der Waals heterostructure are thermodynamically stable. The calculated band structure shows that SnS, SnSe and SnS-SnSe van der Waals heterostructure are indirect band nature while the heterostructure are confirmed for type-II band alignment. Bader charge analysis shows that the charges are transfer from SnS layer to SnSe layer. Furthermore, absorption spectra are calculated to understand the optical behavior of these systems, where the lowest energy transitions are lies in visible region. The valence and conduction band edges straddle the standard redox potentials in SnS, SnSe and their van der Waals heterostructures van der Waals heterostructures, making them promising candidates for water splitting in the acidic solution.

## 1. Introduction

Since the discovery of graphene, new two-dimensional (2D) materials continue to emerge with novel electronic and optoelectronic properties [1–6]. Lots of graphene-like 2D materials, such as boron nitride [7,8], transition metal dichalcogenides (TMDCs) [9], phosphorene [10,11], graphitic carbon nitrides [12–16] and others [17–20] have been widely studied due to their distinctive physical properties and numerous promising applications [21]. Among them, the group IV chalcogenides has received extensive attention due to its rich earth resources, environmental friendliness, low cost, and unique applications in the fields of solar energy conversion, photovoltaics, and thermoelectric devices [22–25]. The most representative Group IV chalcogenide is SnSe, which is a well-known high-performance thermoelectric material with ultra-low thermal conductivity [26,27]. In addition, bulk and monolayer-group IV monochalcogenides MX (M = Ge, Sn; X = S, Se) have many advantages, such as stability, flexibility and high performance as piezoelectric materials. In sharp contrast to MoS<sub>2</sub> and AlN,

the anisotropic piezoelectric coefficient of the MX series is quite large [28,29]. Moreover, the atomically thin Group IV monochalcogenide is of interest as a required spin transport device in spin physics. For example, due to the interaction of spin orbit coupling in SnSe and GeSe sheets, the lack of inversion symmetry and dipole moments are generated, which causes anisotropic energy band spin splitting and makes the sheet dependent on the direction. Aspect has unprecedented potential for spin transmission equipment [30]. In the group IV monochalcogenide family, SnS and SnSe have significant high absorption efficiency because their absorption rate is close to the optical absorption threshold of 1.3 eV [31], which is an optimal band gap.

Recently, there have been many different strategies that can be effectively used to tune the properties of two dimensional materials different techniques such as, external electric field intensity [32,33], strain engineering [34,35], and the normally stacking via van der Waals (vdW) interactions of monolayers [36–39]. Type-II band alignment are achieved by limiting of valence band maximum (VBM), conduction band minimum (CBM) to various layers of vdW heterostructures is

\* Corresponding author.

E-mail addresses: [dothinga@tdtu.edu.vn](mailto:dothinga@tdtu.edu.vn) (T.-N. Do), [lethihoa8@duytan.edu.vn](mailto:lethihoa8@duytan.edu.vn) (L.T. Hoa).

capable to modulate the transition energy of the interlayer and responsible for charge separation [40], hence intensively uses in designing advanced optoelectronic devices [41].

Vertical stacking of combining distinct 2D materials in the form of heterostructures has useful technique to modulate the structure and electronic properties of 2D materials. Which give exciting physical properties which play key role in nanoscale, electronic and photovoltaic devices [42–46]. One of the unique properties of van der Waals (vdW) interaction is type-II band alignment, in which CBM and VBM is due to the different monolayers from the heterostructures [47,48]. Generally, when two different monolayers combined to form type-II heterojunctions the VB and CB of materials A are normally higher than semiconductor of B, so the generated electrons will move from the CBM of A to the VBM of B monolayer with lower reduction potential, while the corresponding holes in the VBM of monolayer B will transfer to monolayer A which have lower oxidation potential, thus a spatial separation of electron and holes pairs will be generated. Also the type-II band alignment is the effective for improving the photocatalytic performance of two dimensional materials [49,50]. BlueP-SiC and arsenene/MoTe<sub>2</sub> [51,52] vdW heterostructures studies show that the type-II band alignment can enhanced the photocatalytic response for water splitting for pH = 0 and also shows good response for optical properties.

In this work, we used first principle calculation to invistigate the properties of SnS and SnSe monolayers and their corresponding heterostructures for the first time. We check the stability by using the AIMD method, which results all SnS and SnSe monolayers and their corresponding heterostructures are thermodynamically stable. After that we find the electronic band structures, band edge alignments, charge transfers, optical properties and photocatalytics properties of SnS and SnSe monolayers and their corresponding heterostructures. Our results present that SnS and SnSe monolayers and their corresponding heterostructures could be a promising material for visible light photocatalysis and electronic and optoelectronic devices.

## 2. Computational details

In present work we used Density functional theory which is implemented in Vienna ab initio simulation package (VASP) [53–57] with the projector augment wave (PAW) method. A vacuum layer of 25 Å is added along the z direction to prevent the periodic boundary conditions. For geometric relaxation we used the Perdew-Burke-Ernzerhof (PBE) functional [58], as its well-known that PBE underestimate the bandgap that is why we used the HSE06 (Heyd-Scuseria-Ernzerhof) functional [59] for electronic structure calculations. The GW<sub>0</sub> method, where only eigenvalues of the Green's function  $G$  are updated, is used for the optical properties of these systems with the help of Bethe–Salpeter equation [60,61]. The  $\Gamma$ -centered Monkhorst–Pack k-meshes of  $6 \times 6 \times 1$  were used for the structural relaxation. The plane wave cutoff was set to 550 eV. A convergence criterion of  $10^{-4}$  eV/Å and  $10^{-5}$  eV for force and energy was adopted, respectively.

## 3. Results and discussions

The optimized atomic structures of SnS and SnSe monolayers are presented in Fig. 1. The lattice constant, band gap and bond length of SnS and SnSe monolayers are given in Table 1. The bond length and lattice constant are 2.61 Å and 3.80 Å for SnS monolayer, while for SnSe are 2.74 Å and 3.91 Å, respectively, which are in good agreement with the available data [62]. Moreover, the thermal stability shows that these monolayers are stable even at room temperature, as depicted in Fig. 2. The band structures calculated by HSE06 method of both SnS and SnSe monolayers are plotted in Fig. 3. We can find that these monolayers are indirect band nature with VBM and CBM at different points. The calculated band gap values of SnS and SnSe monolayers are 2.89 eV and 2.65 eV, respectively, agreed well with available data [62].

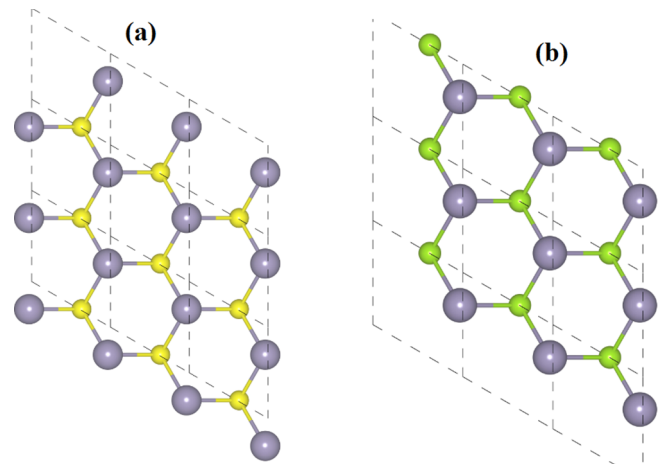


**Fig. 1.** Top view of SnS and SnSe monolayers, where yellow, green and blue balls represent S, Se and Sn atoms respectively.

**Table 1**

Lattice constant ( $a$ ), bond length (M-X), band gap ( $E_g$ ), conduction and valence band edge potentials ( $E_{CB}$ ,  $E_{VB}$ ), binding energy ( $E_b$ ), interlayer distance ( $d$ ) of the SnS, SnSe monolayer and the SnS-SnSe heterostructure.

	SnS	SnSe	SnS-SnSe
$a$ (Å)	3.80	3.91	3.85
S-Sn (Å)	2.61	2.74	2.57
Sn-Se (Å)	—	—	2.78
$E_g$ (PBE) (eV)	—	—	0.67
$E_g$ (PBE + SOC) (eV)	—	—	0.60
$E_g$ (HSE) (eV)	2.89	2.65	1.50
$E_b/d$ (stacking-1) (eV/Å)	—	—	−0.466/3.309
$E_b/d$ (stacking-2) (eV/Å)	—	—	−0.426/3.314
$E_b/d$ (stacking-3) (eV/Å)	—	—	−0.423/3.871
$E_{CB}$ (eV)	−0.214	−0.195	−0.102
$E_{VB}$ (eV)	2.122	2.054	1.560

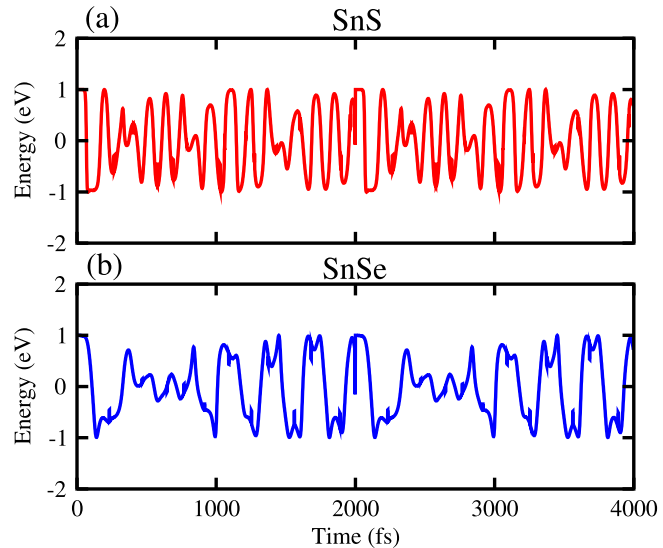


**Fig. 2.** The fluctuation of total energies of (a) SnS and (b) SnSe monolayers, performing by ab initio molecular dynamics simulation at room temperature.

Weighted band structure shows that for SnS the main contribution in VBM is due to the S state while CBM is due to the Sn state. The similar trend is also for SnSe in which VBM is due to the S state while CBM is due to the Sn state, as depicted in Fig. 4.

We now turn to construct the SnS-SnSe heterostructures using the

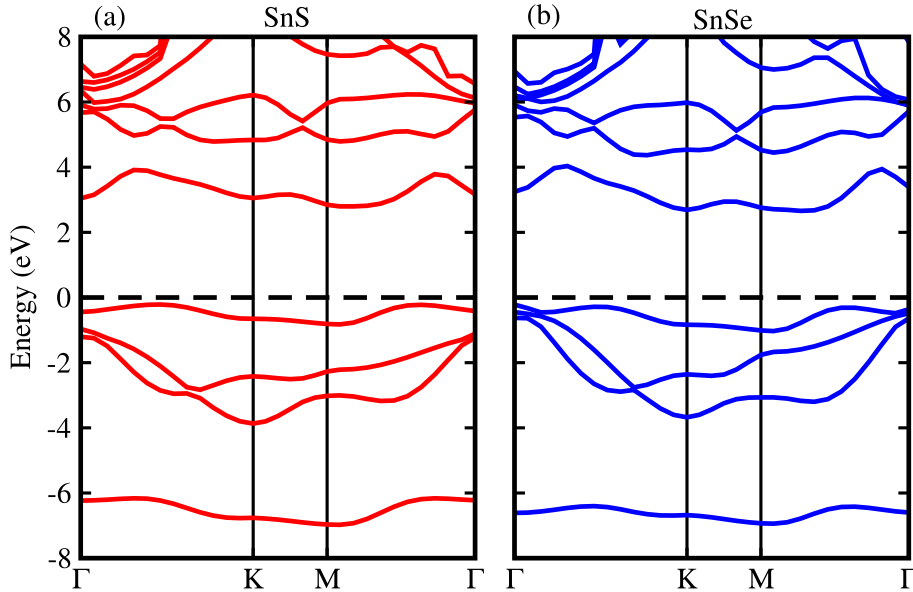


**Fig. 3.** Electronic band structure of (a) SnS and (b) SnSe monolayers, respectively. The dashed black line represents the Fermi level and set to be zero.

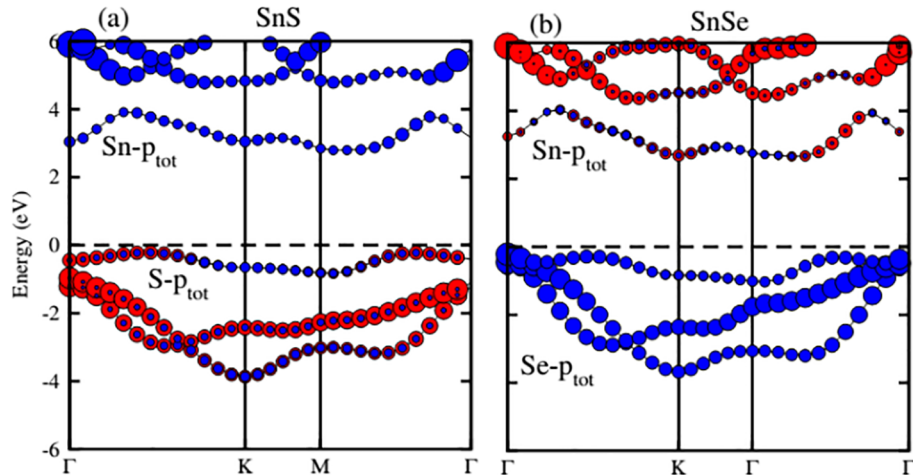


**Fig. 4.** Weighted band structures of (a) SnS and (b) SnSe monolayers.

supercell method. Here, we studied three possible stacking for SnS-SnSe heterostructures, as illustrated in Fig. 5. For stacking-1, Sn atom is on the top of Sn atom, while S atom is on the top of Se atom. For stacking-2, Sn atom is on the top of Sn atom, while S atom is on the hexagonal ring. In stacking-3, S atom is on the top of Se atom, while Sn is on the hexagonal ring. Based on the binding energies and interlayer distances, we can find that the more negative binding energy and smaller interlayer distance the most stable stacking becomes. Binding energy is calculated by the difference of the total energy from the corresponding heterostructures and their constituent monolayers:  $E_b = E_H - E_{SnS} - E_{SnSe}$ . Here,  $E_H$  represents the total energy of SnS-SnSe heterostructure. The  $E_{SnS}$  and  $E_{SnSe}$  are the total energies of SnS and SnSe monolayers, respectively. The calculated binding energy and the interlayer distance for all stacking configuration are presented in Table 1. Among different stacking configurations, one can find that the stacking-1 is the most energetically favorable configuration due to its smallest binding energy and shortest interlayer distance in SnS-SnSe heterostructures. Therefore, the stacking-1 is examined in our next calculations. Moreover, to check the thermal stability of such stacking configuration, we further perform ab initio molecular dynamics calculations after 4 ps. These results are depicted in Fig. 6. One can see that there are small fluctuations in the total energy of SnS-SnSe heterostructure before and after

heating 4 ps. In addition, we can find that is no geometric reconstruction or bonds broken after heating 4 ps at room temperature. All these findings confirm the thermally stable of such SnS-SnSe heterostructure.

The band structures of SnS-SnSe heterostructure using PBE, PBE + SOC and HSE06 method are presented in Fig. 7. It can be seen that the band nature of SnS-SnSe heterostructure is indirect. The band gap calculated by PBE is 0.67 eV, while it decreases to 0.60 eV by using PBE + SOC. The nature of such decrease is due to the appearance in the band splitting when the SOC effect is induced. As the PBE method underestimated the band gap values, so here we also used the HSE06 method to give the correct band gap of SnS-SnSe heterostructure. The HSE06 band gap of SnS-SnSe heterostructure is calculated to be 1.50 eV.

To check for the band alignment types of such SnS-SnSe heterostructure, we also calculate and plot the weighted band structure of SnS-SnSe heterostructure, as depicted in Fig. 8(a). We find the VBM of SnS-SnSe heterostructure is due to the S-p<sub>z</sub> state of SnS layer, whereas the CBM comes from the Sn-p<sub>z</sub> state of SnSe layer. Therefore, the SnS-SnSe heterostructure depicts the type-II band alignment, revealing remarkable applications in optoelectronic and photovoltaic applications due to the efficient electron-hole separation. Moreover, the SnS-SnSe heterostructure exhibits an indirect semiconductor. Such characteristics

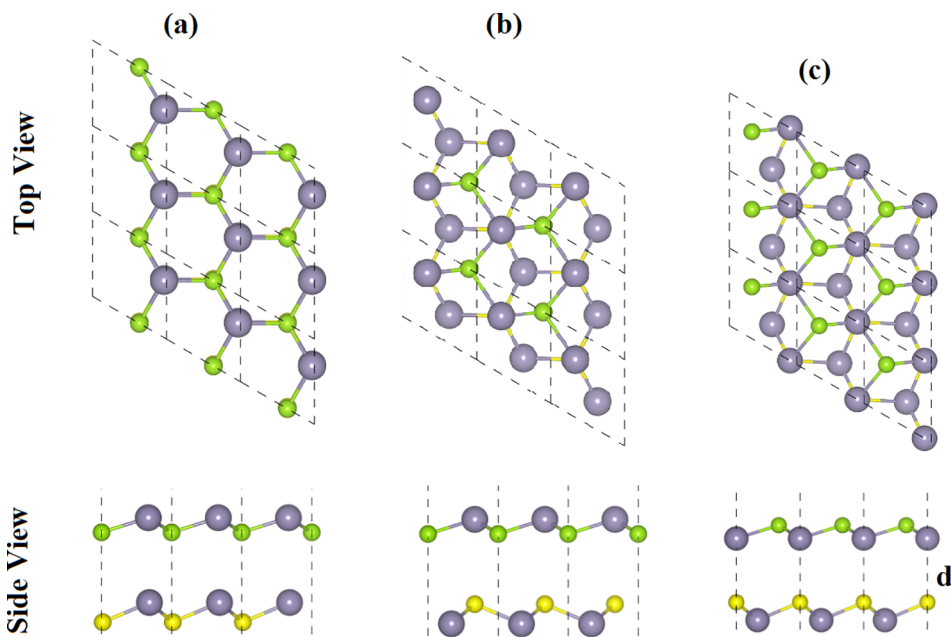


**Fig. 5.** Different possible stacking of SnS-SnSe heterostructures. Yellow and green balls stand for S and Se atoms, while blue balls represent the Sn atoms.

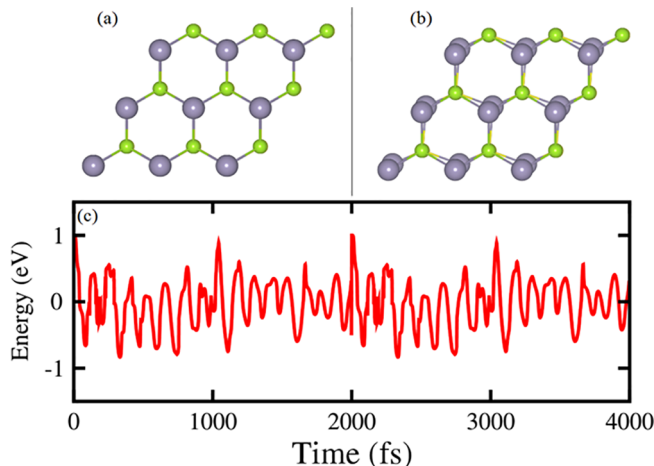


**Fig. 6.** (a) and (b) represent the SnS-SnSe heterostructure before and after heating the system, respectively. (c) The fluctuation of the total energy of SnS-SnSe heterostructure for stacking-1 pattern as a function of the time step.

in band structures will spontaneously separate the free electrons and holes, enabling the high efficiency optoelectronics and solar energy conversions [63,64].

To have a better understanding the charge distribution in SnS-SnSe heterostructure, we further visualize the charge density difference, which can be calculated as follows:  $\Delta\rho = \rho_H - \rho_{SnS} - \rho_{SnSe}$ , where  $\rho_H$  is the charge density of SnS-SnSe heterostructure. The  $\rho_{SnS}$  and  $\rho_{SnSe}$  are the charge densities of SnS and SnSe monolayers, respectively. Such result is depicted in Fig. 8(b). Bader population analysis shows that in SnS-SnSe heterostructure, 0.14 e per unit cell charges are transferred from SnS monolayer to SnSe monolayer. Hence, SnS become p-doping, while SnSe become n-doping. The photogenerated free charge carriers are effectively separated, indicating these vdW heterostructures for prominent applications in solar energy conversion [64].

Furthermore, in order to examine the optical performance of SnS-SnSe heterostructure for practical applications, we also calculate its optical properties along with those of the constituent monolayers. The imaginary part of dielectric function of SnS-SnSe heterostructure and the corresponding monolayers is depicted in Fig. 9. One can see that the SnS-SnSe heterostructure has a high optical absorption as compared with the constituent SnS and SnSe monolayers. In addition, all peaks in

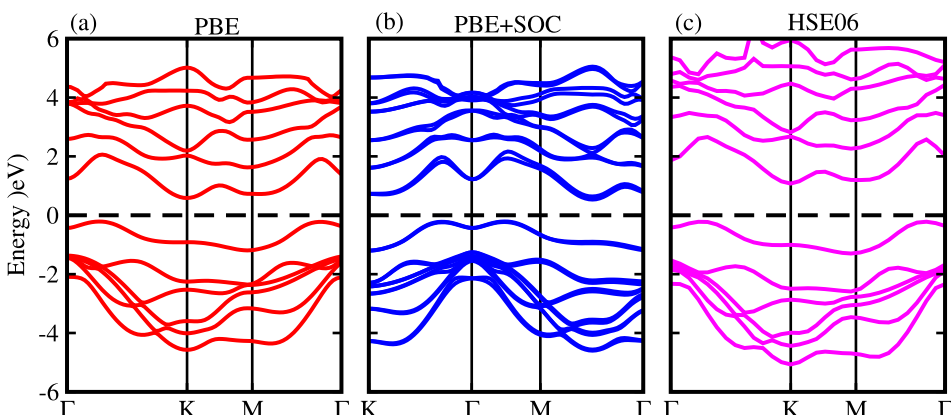


**Fig. 7.** Band structures of SnS-SnSe heterostructures using (a) PBE, (b) PBE + SOC and (c) HSE06 methods, respectively.

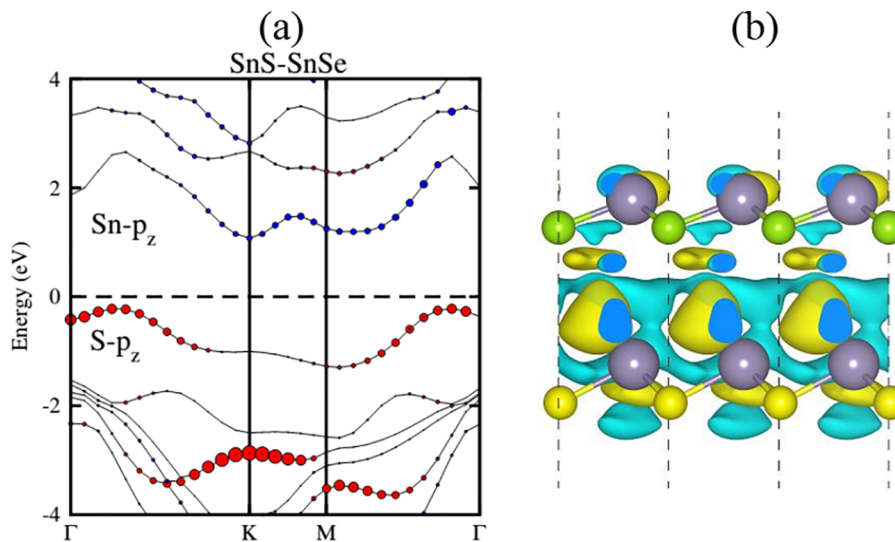


**Fig. 8.** (a) Weighted band structure of SnS-SnSe heterostructures using HSE06 method. (b) Charge density difference of SnS-SnSe heterostructure. The yellow and cyan areas represent the charge accumulation and depletion, respectively.

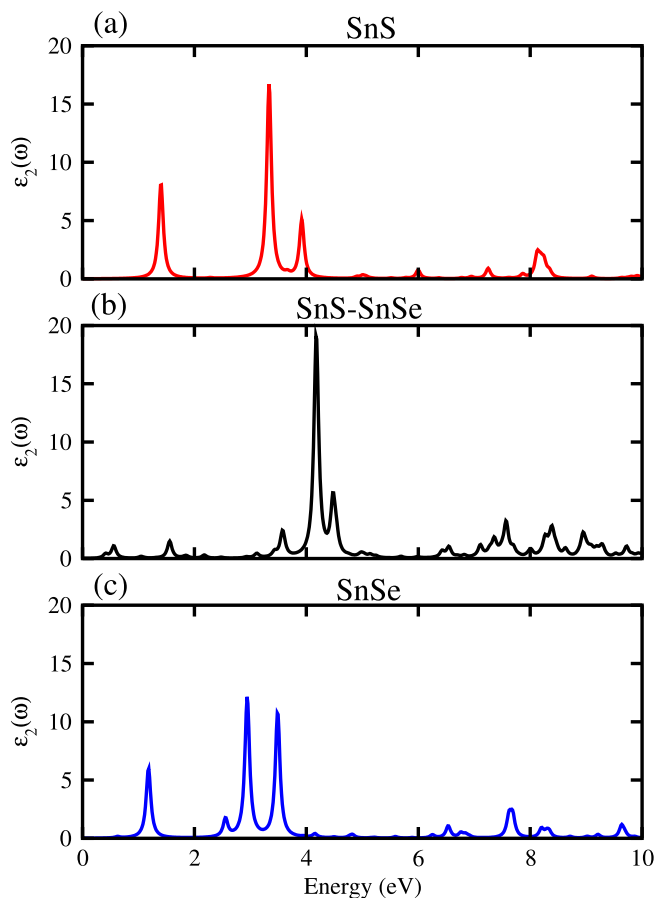


**Fig. 9.** Imaginary part of dielectric function of the constituent (a) SnS, (c) SnSe monolayer and (b) their corresponding SnS-SnSe heterostructure.

the optical spectrum of the SnS-SnSe heterostructure are appeared in visible region.

The photocatalytic water splitting for the SnS and SnSe monolayers and their corresponding heterostructures are investigated by using Mulliken electronegativity  $E_{VBM} = -E_{elec} + 0.5 \times E_g$  and  $E_{CBM} = E_{VBM} - E_g$  for pH = 0 [65,66]. One can find from Fig. 10 that the CBM and VBM edges of SnS and SnSe monolayers cover the required

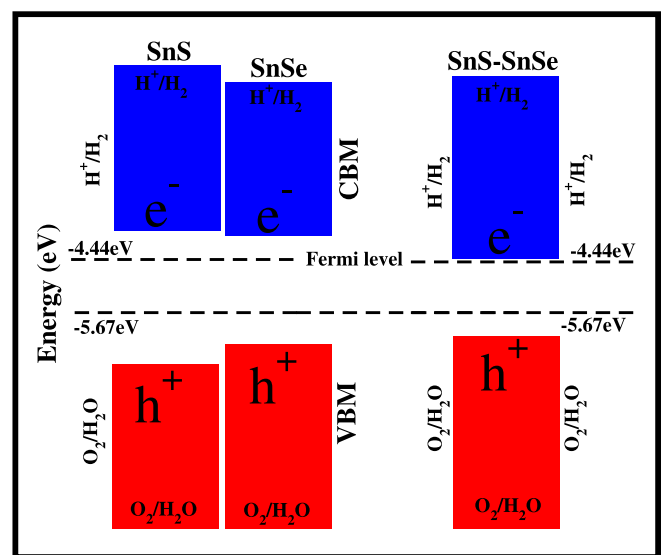


**Fig. 10.** Valence and conduction band edges for SnS and SnSe monolayers and their heterostructures. The blue and red colors represent the CBM and VBM of semiconductors, respectively.

redox potentials, indicating the ability for oxidation and reduction of water at pH = 0. Moreover, the SnS-SnSe heterostructure also exhibits the power to split water to O<sub>2</sub> and H<sup>+</sup>, hence showing good response for photocatalysts. Therefore, we can conclude that SnS, SnSe monolayers and their SnS-SnSe heterostructure are highly efficient photocatalysts for conversion of solar light into hydrogen, which is an attractive technique for the production of clean and renewable energy device applications.

#### 4. Conclusion

In summary, we have investigated the structural, electronic, optical and photocatalytic properties of SnS, SnSe and their heterostructure by first principles calculations. Our result shows that the SnS, SnSe and their heterostructure are energetically and dynamically feasible. The SnS-SnSe vdW heterostructure shows indirect band nature with type-II band alignment. Bader charge analysis and charge density difference confirm that SnS layer donates electrons to the SnSe layer. More

importantly, SnS-SnSe vdW heterostructure show obvious absorption peaks in the visible region, which leads to the efficient use of solar energy. The CB and VB edges for both models straddle the standard redox potentials which shows good response for water splitting and are useful for dissociating water into  $H^+$ /H<sub>2</sub> and O<sub>2</sub>/H<sub>2</sub>O. We expect that the obtained results can provide a valuable guidance for synthesis of SnS-SnSe vdW heterostructure for potential applications as photocatalysts.

### CRediT authorship contribution statement

**Thi-Nga Do:** Investigation, Software, Conceptualization, Validation. **M. Idrees:** Conceptualization, Software, Investigation. **Bin Amin:** Investigation, Validation, Supervision, Funding acquisition. **Nguyen N. Hieu:** Methodology, Investigation, Validation. **Huynh V. Phuc:** Methodology, Investigation, Validation. **Le T. Hoa:** Conceptualization, Writing - review & editing. **Chuong V. Nguyen:** Conceptualization, Supervision, Writing - original draft, Writing - review & editing.

### Declaration of Competing Interest

The authors declare that they have no known competing financial interests or personal relationships that could have appeared to influence the work reported in this paper.

### Acknowledgement

This research is supported from the Higher Education Commission of Pakistan (HEC) under Project No. 5727/261 KPK/NRPU/R&D/HEC2016.

### References

- [1] V. Nicolosi, M. Chhowalla, M.G. Kanatzidis, M.S. Strano, J.N. Coleman, Liquid exfoliation of layered materials, *Science* 340 (6139).
- [2] D. Akinwande, N. Petrone, J. Hone, Two-dimensional flexible nanoelectronics, *Nature Commun.* 5 (1) (2014) 1–12.
- [3] X. Rui, Z. Lu, H. Yu, D. Yang, H.H. Hng, T.M. Lim, Q. Yan, Ultrathin v 2 o 5 nanosheet cathodes: realizing ultrafast reversible lithium storage, *Nanoscale* 5 (2) (2013) 556–560.
- [4] J.N. Coleman, M. Lotya, A. O'Neill, S.D. Bergin, P.J. King, U. Khan, K. Young, A. Gaucher, S. De, R.J. Smith, et al., Two-dimensional nanosheets produced by liquid exfoliation of layered materials, *Science* 331 (6017) (2011) 568–571.
- [5] H. Liu, A.T. Neal, Z. Zhu, Z. Luo, X. Xu, D. Tománek, P.D. Ye, Phosphorene: an unexplored 2d semiconductor with a high hole mobility, *ACS Nano* 8 (4) (2014) 4033–4041.
- [6] M. Dávila, L. Xian, S. Cahangirov, A. Rubio, G. Le Lay, Germanene: a novel two-dimensional germanium allotrope akin to graphene and silicene, *New J. Phys.* 16 (9) (2014) 095002.
- [7] J. Nakamura, T. Nitta, A. Natori, Electronic and magnetic properties of bnc ribbons, *Phys. Rev. B* 72 (20) (2005) 205429.
- [8] A. Du, S.C. Smith, G. Lu, First-principle studies of electronic structure and c-doping effect in boron nitride nanoribbon, *Chem. Phys. Lett.* 447 (4–6) (2007) 181–186.
- [9] Y. Li, Z. Zhou, S. Zhang, Z. Chen, MoS<sub>2</sub> nanoribbons: high stability and unusual electronic and magnetic properties, *J. Am. Chem. Soc.* 130 (49) (2008) 16739–16744.
- [10] L. Li, Y. Yu, G.J. Ye, Q. Ge, X. Ou, H. Wu, D. Feng, X.H. Chen, Y. Zhang, Black phosphorus field-effect transistors, *Nature Nanotechnol.* 9 (5) (2014) 372.
- [11] H.O. Churchill, P. Jarillo-Herrero, Phosphorus joins the family, *Nature Nanotechnol.* 9 (5) (2014) 330–331.
- [12] A. Bafecky, M. Neek-Amal, Tuning the electronic properties of graphene-graphitic carbon nitride heterostructures and heterojunctions by using an electric field, *Phys. Rev. B* 101 (8) (2020) 085417.
- [13] A. Bafecky, C. Stampfl, B. Akgenc, B. Mortazavi, M. Ghergherehchi, C.V. Nguyen, Embedding of atoms into the nanopore sites of the c6n6 and c6n8 porous carbon nitride monolayers with tunable electronic properties, *Phys. Chem. Chem. Phys.* 22 (2020) 6418–6433.
- [14] A. Bafecky, M. Neek-Amal, F. Peeters, Two-dimensional graphitic carbon nitrides: Strain-tunable ferromagnetic ordering, *Phys. Rev. B* 101 (16) (2020) 165407.
- [15] A. Bafecky, Graphene-like bc6n single-layer: Tunable electronic and magnetic properties via thickness, gating, topological defects, and adatom/molecule, *Physica E* 118 (2020) 113850.
- [16] A. Bafecky, C. Stampfl, B. Akgenc, M. Ghergherehchi, Control of c 3 n 4 and c 4 n 3 carbon nitride nanosheets' electronic and magnetic properties through embedded atoms, *PCCP* 22 (4) (2020) 2249–2261.
- [17] D.J. Late, B. Liu, J. Luo, A. Yan, H.R. Matte, M. Grayson, C. Rao, V.P. Dravid, Gas and gase ultrathin layer transistors, *Adv. Mater.* 24 (26) (2012) 3549–3554.
- [18] Q. Tang, Z. Zhou, Graphene-analogous low-dimensional materials, *Progress Mater. Sci.* 58 (8) (2013) 1244–1315.
- [19] Q. Tang, Z. Zhou, Z. Chen, Innovation and discovery of graphene-like materials via density-functional theory computations, *Wiley Interdisciplinary Rev.: Comput. Mol. Sci.* 5 (5) (2015) 360–379.
- [20] A. Bafecky, C. Stampfl, F.M. Peeters, Dirac half-metallicity of thin pdcl 3 nanosheets: Investigation of the effects of external fields, surface adsorption and defect engineering on the electronic and magnetic properties, *Sci. Rep.* 10 (1) (2020) 1–15.
- [21] F. Shoaiei, J.R. Hahn, H.S. Kang, Electronic structure and photocatalytic band offset of few-layer gap 2, *J. Mater. Chem. A* 5 (42) (2017) 22146–22155.
- [22] L. Li, Z. Chen, Y. Hu, X. Wang, T. Zhang, W. Chen, Q. Wang, Single-layer single-crystalline snse nanosheets, *J. Am. Chem. Soc.* 135 (4) (2013) 1213–1216.
- [23] P.D. Antunez, J.J. Buckley, R.L. Brutcher, Tin and germanium monochalcogenide iv–vi semiconductor nanocrystals for use in solar cells, *Nanoscale* 3 (6) (2011) 2399–2411.
- [24] D.-J. Xue, J. Tan, J.-S. Hu, W. Hu, Y.-G. Guo, L.-J. Wan, Anisotropic photoresponse properties of single micrometer-sized gese nanosheet, *Adv. Mater.* 24 (33) (2012) 4528–4533.
- [25] H. Wang, Y. Gao, G. Liu, Anisotropic phonon transport and lattice thermal conductivities in tin dichalcogenides sns 2 and snse 2, *RSC Adv.* 7 (14) (2017) 8098–8105.
- [26] G. Tan, L.-D. Zhao, F. Shi, J.W. Doak, S.-H. Lo, H. Sun, C. Wolverton, V.P. Dravid, C. Uher, M.G. Kanatzidis, High thermoelectric performance of p-type snte via a synergistic band engineering and nanostructuring approach, *J. Am. Chem. Soc.* 136 (19) (2014) 7006–7017.
- [27] Z.-Y. Hu, K.-Y. Li, Y. Lu, Y. Huang, X.-H. Shao, High thermoelectric performances of monolayer snse allotropes, *Nanoscale* 9 (41) (2017) 16093–16100.
- [28] K. Hippalgaonkar, Y. Wang, Y. Ye, D.Y. Qiu, H. Zhu, Y. Wang, J. Moore, S.G. Louie, X. Zhang, High thermoelectric power factor in two-dimensional crystals of mo s 2, *Phys. Rev. B* 95 (11) (2017) 115407.
- [29] Z. Nabi, A. Kellou, S. Mecabih, A. Khalfi, N. Benosman, Opto-electronic properties of rutile sno2 and orthorhombic sns and snse compounds, *Mater. Sci. Eng.: B* 98 (2) (2003) 104–115.
- [30] G. Shi, E. Kioupakis, Anisotropic spin transport and strong visible-light absorbance in few-layer snse and gese, *Nano Lett.* 15 (10) (2015) 6926–6931.
- [31] K.R. Reddy, N.K. Reddy, R. Miles, Photovoltaic properties of sns based solar cells, *Solar Energy Mater. Solar Cells* 90 (18–19) (2006) 3041–3046.
- [32] J. Shang, S. Zhang, X. Cheng, Z. Wei, J. Li, Electric field induced electronic properties modification of zrs 2/hfs 2 van der waals heterostructure, *RSC Adv.* 7 (24) (2017) 14625–14630.
- [33] A. Bafecky, C. Stampfl, F.M. Peeters, The electronic, optical, and thermoelectric properties of monolayer pbte and the tunability of the electronic structure by external fields and defects, *physica status solidi (b)* (2020) 2000182.
- [34] J. Shang, S. Zhang, X. Cheng, Z. Wei, J. Li, Electric field induced electronic properties modification of zrs 2/hfs 2 van der waals heterostructure, *RSC Adv.* 7 (24) (2017) 14625–14630.
- [35] A. Bafecky, B. Akgenc, M. Ghergherehchi, F. Peeters, Strain and electric field tuning of semi-metallic character wrco2mxenes with dual narrow band gap, *J. Phys.: Condens. Matter* 32 (35) (2020) 355504.
- [36] T. Roy, M. Tosun, X. Cao, H. Fang, D.-H. Lien, P. Zhao, Y.-Z. Chen, Y.-L. Chueh, J. Guo, A. Javey, Dual-gated mos2/wse2 van der waals tunnel diodes and transistors, *ACS Nano* 9 (2) (2015) 2071–2079.
- [37] A. Bafecky, M. Yagmurkucukardes, B. Akgenc, M. Ghergherehchi, C.V. Nguyen, Van der waals heterostructures of mos2 and janus mosse monolayers on graphitic boron-carbon-nitride (bc 3, c 3 n, c3n4 and c4n3) nanosheets: a first-principles study, *J. Phys. D: Appl. Phys.* 53 (35) (2020) 355106.
- [38] O. Lopez-Sanchez, E. Alarcon Llado, V. Koman, A. Fontcuberta i Morral, A. Radenovic, A. Kis, Light generation and harvesting in a van der waals heterostructure, *Acs Nano* 8 (3) (2014) 3042–3048.
- [39] A. Bafecky, C. Stampfl, M. Ghergherehchi, Strain, electric-field and functionalization induced widely tunable electronic properties in mos2/bc3/c3n and/c3n4 van der waals heterostructures, *Nanotechnology* 31 (29).
- [40] Z. Yu, Y. Pan, Y. Shen, Z. Wang, Z.-Y. Ong, T. Xu, R. Xin, L. Pan, B. Wang, L. Sun, et al., Towards intrinsic charge transport in monolayer molybdenum disulfide by defect and interface engineering, *Nature Commun.* 5 (1) (2014) 1–7.
- [41] P. Rivera, J.R. Schaibley, A.M. Jones, J.S. Ross, S. Wu, G. Aivazian, P. Klement, K. Seyler, G. Clark, N.J. Ghimire, et al., Observation of long-lived interlayer excitons in monolayer mose 2-wse 2 heterostructures, *Nature Commun.* 6 (1) (2015) 1–6.
- [42] X. Hong, J. Kim, S.-F. Shi, Y. Zhang, C. Jin, Y. Sun, S. Tongay, J. Wu, Y. Zhang, F. Wang, Ultrafast charge transfer in atomically thin mos 2/ws 2 heterostructures, *Nature Nanotechnol.* 9 (9) (2014) 682–686.
- [43] L. Wang, I. Meric, P. Huang, Q. Gao, Y. Gao, H. Tran, T. Taniguchi, K. Watanabe, L. Campos, D. Muller, et al., One-dimensional electrical contact to a two-dimensional material, *Science* 342 (6158) (2013) 614–617.
- [44] B. Amin, T.P. Kaloni, U. Schwingenschlögl, Strain engineering of ws 2, wse 2, and wte 2, *Rsc Adv.* 4 (65) (2014) 34561–34565.
- [45] Q. Sun, Y. Dai, Y. Ma, W. Wei, B. Huang, Vertical and bidirectional heterostructures from graphyne and mse2 (m = mo, w), *J. Phys. Chem. Lett.* 6 (14) (2015) 2694–2701.
- [46] W. Xia, L. Dai, P. Yu, X. Tong, W. Song, G. Zhang, Z. Wang, Recent progress in van der waals heterojunctions, *Nanoscale* 9 (13) (2017) 4324–4365.
- [47] K.D. Pham, N.N. Hieu, H.V. Phuc, I. Fedorov, C. Duque, B. Amin, C.V. Nguyen, Layered graphene/gas van der waals heterostructure: Controlling the electronic

- properties and schottky barrier by vertical strain, *Appl. Phys. Lett.* 113 (17) (2018) 171605.
- [48] L. Lin, S. Li, W. Yu, L. Zhu, J. Huang, Z. Zhang, H. Tao, W.-B. Zhang, Electronic structures and strain responses of group va/va two-dimensional van der waals heterostructures, *Vacuum* 109296 (2020).
- [49] A.A. Isari, A. Payan, M. Fattah, S. Jorfi, B. Kakavandi, Photocatalytic degradation of rhodamine b and real textile wastewater using fe-doped tio<sub>2</sub> anchored on reduced graphene oxide (fe-tio<sub>2</sub>/rgo): characterization and feasibility, mechanism and pathway studies, *Appl. Surf. Sci.* 462 (2018) 549–564.
- [50] M.T. Uddin, Y. Nicolas, C. Olivier, T. Toupane, L. Servant, M.M. Muller, H.-J. Kleebe, J. Ziegler, W. Jaegermann, Nanostructured sno<sub>2</sub>-zno heterojunction photocatalysts showing enhanced photocatalytic activity for the degradation of organic dyes, *Inorg. Chem.* 51 (14) (2012) 7764–7773.
- [51] M. Idrees, H. Din, S. Khan, I. Ahmad, L.-Y. Gan, C.V. Nguyen, B. Amin, Van der waals heterostructures of p, bse, and sic monolayers, *J. Appl. Phys.* 125 (9) (2019) 094301.
- [52] J. Liu, M. Xue, J. Wang, H. Sheng, G. Tang, J. Zhang, D. Bai, Tunable electronic and optical properties of arsenene/mote<sub>2</sub> van der waals heterostructures, *Vacuum* 163 (2019) 128–134.
- [53] W. Kohn, L.J. Sham, Self-consistent equations including exchange and correlation effects, *Phys. Rev.* 140 (4A) (1965) A1133.
- [54] G. Kresse, J. Hafner, Ab initio molecular dynamics for open-shell transition metals, *Phys. Rev. B* 48 (17) (1993) 13115.
- [55] P.E. Blöchl, Projector augmented-wave method, *Phys. Rev. B* 50 (24) (1994) 17953.
- [56] S. Grimme, Semiempirical gga-type density functional constructed with a long-range dispersion correction, *J. Comput. Chem.* 27 (15) (2006) 1787–1799.
- [57] S. Barraza-Lopez, T.P. Kaloni, S.P. Poudel, P. Kumar, Tuning the ferroelectric-to-paraelectric transition temperature and dipole orientation of group-iv monochalcogenide monolayers, *Phys. Rev. B* 97 (2) (2018) 024110.
- [58] J.P. Perdew, K. Burke, M. Ernzerhof, Generalized gradient approximation made simple, *Phys. Rev. Lett.* 77 (18) (1996) 3865.
- [59] J. Heyd, G.E. Scuseria, M. Ernzerhof, Hybrid functionals based on a screened coulomb potential, *J. Chem. Phys.* 118 (18) (2003) 8207–8215.
- [60] M. Shishkin, G. Kresse, Implementation and performance of the frequency-dependent gw method within the paw framework, *Phys. Rev. B* 74 (3) (2006) 035101.
- [61] M. Rohlfing, S.G. Louie, Electron-hole excitations in semiconductors and insulators, *Phys. Rev. Lett.* 81 (11) (1998) 2312.
- [62] C. Kamal, A. Chakrabarti, M. Ezawa, Direct band gaps in group iv-vi monolayer materials: Binary counterparts of phosphorene, *Phys. Rev. B* 93 (12) (2016) 125428.
- [63] Q. Peng, Z. Wang, B. Sa, B. Wu, Z. Sun, Electronic structures and enhanced optical properties of blue phosphorene/transition metal dichalcogenides van der waals heterostructures, *Sci. Rep.* 6 (2016) 31994.
- [64] V.D.S. Ganesan, J. Linghu, C. Zhang, Y.P. Feng, L. Shen, Heterostructures of phosphorene and transition metal dichalcogenides for excitonic solar cells: A first-principles study, *Appl. Phys. Lett.* 108 (12) (2016) 122105.
- [65] T.R. Cook, D.K. Dogutan, S.Y. Reece, Y. Surendranath, T.S. Teets, D.G. Nocera, Solar energy supply and storage for the legacy and nonlegacy worlds, *Chem. Rev.* 110 (11) (2010) 6474–6502.
- [66] A. Kudo, Y. Miseki, Heterogeneous photocatalyst materials for water splitting, *Chem. Soc. Rev.* 38 (1) (2009) 253–278.